Journal of Sciences, Islamic Republic of Iran 20(4): 331-342 (2009) http://jsciences.ut.ac.ir
University of Tehran, ISSN 1016-1104

Geochemistry and Tectonic Setting of Pleistocene Basaltic Lava Flows in the Shahre-Babak Area, NW of Kerman, Iran: Implication for the Evolution of Urumieh-Dokhtar Magmatic Assemblage

S.Z. Hosseini,[1,*] M. Arvin,[1] R. Oberhansli,[2] and S. Dargahi[1]

[1] *Department of Geology, Shahid Bahonar University of Kerman, P.O. Box 76175-133 Kerman, Islamic Republic of Iran*
[2] *Department of Geology, Potsdam University, P.O. Box 601553-14415 Potsdam, Germany*

Received: 2 February 2009 / Revised: 29 August 2009 / Accepted: 29 November 2009

Abstract

Pleistocene basaltic lava flows, consisting of trachybasalt and basaltic trachyandesite, cover an area north-northwest of Shahre-Babak in southeastern Iran. The whole rock chemistry indicates that the lavas are dominantly alkaline and mildly calc-alkaline. Variation diagrams of SiO_2 with major and trace elements are consistent with fractional crystallization processes involving olivine, pyroxene, plagioclase, ± hornblende and Fe-Ti oxides. In both rock types trace element variations show similar high LILE/HFSE ratios, which along with their similar fractionation trend, implying a common magma source but different degrees of evolution. Their MORB normalized incompatible trace element concentrations show enrichment in LILE (e.g., Sr, K, Rb, Ba) and LREE (e.g., Ce), but depletion in HFSE (e.g., Ta, Nb, Ti, Zr, Hf, Y) and HREE (e.g. Yb). The Shahre-Babak alkaline basalts show characteristics of subduction related (active) continental margins, OIB and within-plate tectonic environments. Regarding the Late Miocene collision time between Arabia and Central Iran, the Shahre-Babak alkaline basaltic lavas should be collision related (post-collisional). Their enrichment in LILE and LREE relative to Ta and Nb can be explained either by: (a) presence of a subduction component or addition of an LILE-enriched, Nb-Ta poor fluid component to the mantle wedge or (b) crustal contamination of mantle-derived magmas during their ascent to the surface through assimilation and fractional crystallization (AFC) and or MASH (melting, assimilation, storage and homogenization). The magma erupted in a post-collisional tectonic setting and formed in a within-plate environment between two north-south running faults and is closely related to deep lithospheric fractures.

Keywords: Basalt; Collision zone volcanism; Pleistocene; Iran; Shahre-Babak

Introduction

The Cenozoic geodynamic evolution of Iran has been dominated by continuous subduction of NeoTethys underneath the Central Iranian microcontinent. The north-east ward motion of the Arabian plate during

---

[*] Corresponding author, Tel.: +98(341)3222035, Fax: :+98(341)3222035, E-mail: shosseini@mail.uk.ac.ir

Eocene to Miocene caused extensive subduction related volcanism in the Urumieh-Dokhtar Magmatic Assemblage (UDMA), a part of the Zagros orogenic belt in Iran (e.g., [25, 34, 10, 2, 4, 55] and references there in). Magmatism in the UDMA started in Early Eocene and continued until Pleistocene with peak of volcanism occurred in Middle to Upper Eocene [9,3]. The volcanism has been followed by continental collision between the Iranian and Arabian plates either during or before the Late Miocene time which led to crustal shortening and thickening in the western edge of the Iranian plate with a NW-SE trend compressional regime that continues today [43]. The thickness of the crust is about 45-50 km in western edges of Iranian plate in the Sanadaj-Sirjan zone [46]. Following the collision event volcanism continued in some parts of UDMA markedly as Pleistocene basic volcanism in Shahre-Babak area, NW of Kerman. It has been advocated that the source and affinity of basaltic lavas can be used for better understanding of tectonic evolution [49]. In this study we present for the first time the petrography and geochemical characteristics of the Pleistocene basaltic lava flows in the Shahre-Babak area and discuss their geochemical affinity, their magma source, and the relationship to the regional tectonic patterns.

1-Tectonic History of the Region

The geological and tectonic history of Iran is linked to the evolution of Tethyan Ocean. The Central Iranian microcontinent was detached from Gondwanaland during Permian to Early Triassic time and subsequently attached to Eurasia along the Alborz and Kopeh-Dagh sutures during the Triassic closure of the Paleo-Tethys Ocean [59, 23, 60]. As a result, the Late Paleozoic ophiolites were emplaced in the North and Northeast of Iran (Fig. 1). As the Paleo-Tethys Ocean was closing, rifting along the present Zagros thrust zone took place on the continental plate. This eventually led to the opening of the Neo-Tethys Ocean [8]. The new ocean was expanded during Late Triassic-Early Jurassic, while pelagic marine carbonates were deposited in Zagros orogenic belt. The Zagros orogenic belt of Iran belonging to the extensive Alpine-Himalayan orogenic system, formed as a result of the separation of Arabia from Africa and its subsequent collision with Eurasia. Structurally the Zagros orogenic belt consists of three parallel NW-SE trending units (Fig. 1a). 1. The Zagros fold-thrust belt (ZFTB) is bounded to the northeast by the Main Zagros reverse fault and is proposed to be the suture zone between the Arabian plate and Eurasia. The ZFTB contains a thick and almost continuous sequence of shelf sediments deposited on the 1-2 km thick Infra-Camberian Hormoz salt formation. These sediments, of Paleozoic to Late Tertiary age, are believed to be separated from the Precambrian metamorphic basement by the Hormoz salt layer [3, 1]. 2. The Sanandaj-Sirjan zone (SSZ; [59]) is made of mainly Jurassic, interbedded phyllites and metavolcanics showing a moderate metamorphic imprint except close to large-scale Mesozoic calc-alkaline plutons. These metamorphic rocks are unconformably overlain by the Barremo-Aptian Orbitolina limestones, typical of

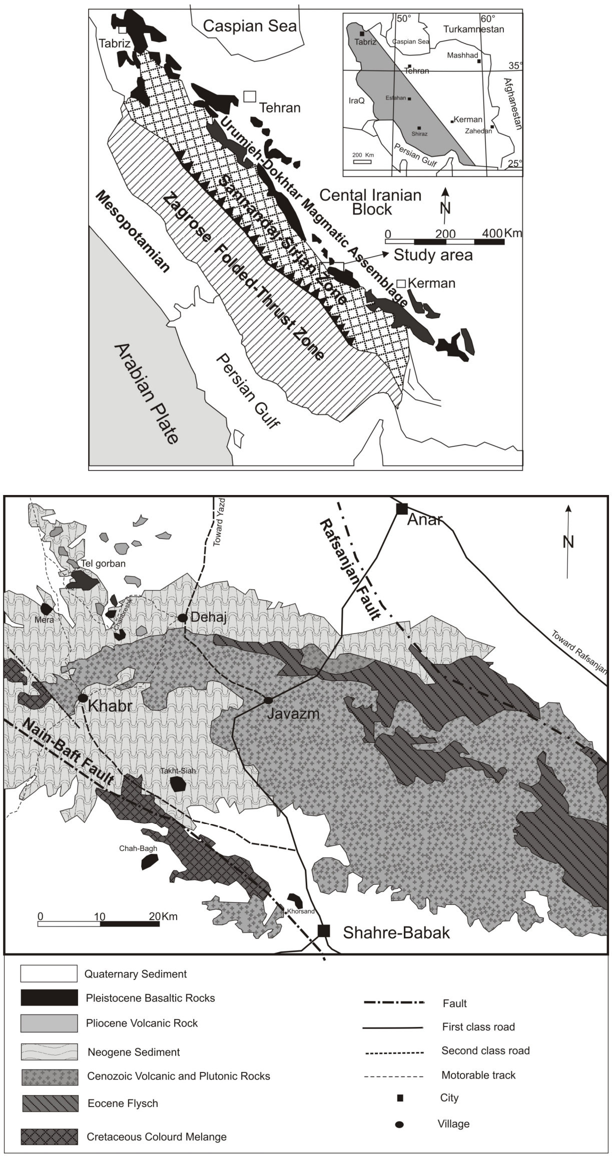

Figure 1. (a) Geological map of Iran illustrating major tectonic units in the Zagros orogenic belt. (b) Simplified geological map of the study area, northeast of Shahre-Babak (modified from Geological map of Iran, 1:100000 Series, Sheet 6951, Dehaj, Dimitrijevic et al., [20]).

Central Iran sedimentation [59]. During most of the second half of the Mesozoic, the SSZ represented an active Andean-like margin whose calc-alkaline magmatic activity progressively shifted northward [9, 54]. 3. The Urumieh-Dokhtar volcanic zone of Schroder [53] or the Urumieh-Dokhtar magmatic assemblage (UDMA) of Alavi [4] is a 150 km wide magmatic assemblage. This magmatic assemblage has been interpreted to be a subduction related Andean type magmatic arc that has been active from the Late Jurassic to present [9, 10]. The UDMA is composed of voluminous tholeiitic, calc-alkaline, and K-rich alkaline intrusive and extrusive rocks (with associated pyroclastic and volcaniclastic successions) along the active margin of the Iranian plates. The oldest rocks in the UDMA are calc-alkaline intrusive rocks, which cut across Upper Jurassic formations and are overlain nonconformably by Lower Cretaceous fossiliferous limestone. The youngest rocks in the UDMA consist of lava flows and pyroclastics that belong to Pliocene to Quaternary volcanic cones of alkaline and calc-alkaline composition [8].

The final closure of Neo-Tethys and collision between Arabian and Central Iranian plates took place before or during Late Miocene [8, 10, 16]. The collision has been purely continental for the past 5 Ma [60, 43, 1]. The convergence velocity of Arabia with respect to Eurasia is approximately 22 ± 2 mm yr^{-1} in the direction N8±°E [67], which has been accommodated by crustal shortening, folding and thrusting deformation in the Zagros, Alborz and Kopeh-Dagh regions and also by lateral displacements of Central Iran blocks along major strike-slip faults [37]. After collision in Late Miocene and as a result of shortening and thickening, volcanic activity continued well into Pleistocene in some parts of UDMA (e.g., basaltic lava flows in Bijar and Shahre-Babak regions, Fig. 1b), leading to formation of alkaline, calc-alkaline volcanic and subvolcanic rocks.

2- Geological Setting

The study area is located on the north-northwest of Shahre-Babak, in the Rafsanjan-Saveh depression which is bounded between two NW-SE running right lateral strike slip faults (Anar and Dehshir faults) and covers about 250 km^2 areas (Fig. 1). According to the Moho map of Dehghani and Makris [18] the crustal thickness of the study area ranges from 48 to 50 km. The Shahre-Babak Pleistocene basaltic lava flows are outcropped to the south of spilitic agglomerates of the ophiolitic "colored mélange" and between the ophiolite and Eocene flysch deposites (Fig. 1). The Tertiary magmatism in the area comprises of two distinct episodes: 1- the Paloegene volcanics which consists of basaltic andesites, latites, analcime rich tephrites, some nepheline phonoliths and volcanicclastic rocks and 2- Oligo-Miocene plutonic rocks consisting of granodiorites, porphyric diorites and porphyric quartz diorite. Late Miocene-Pliocene magmatic activity comprises of some dacitic-andesiic domes and lava flows. In the Shahre-Babak area Pliestocene basaltic lavas, covering Quaternary terraces, were formed through monogenetic volcanic activity and occur as mesa-forming flows. Those confined to the south of UDMA in Chah-Bagh, Takhte-Siah and Khorsand localities are trachybasalts, whereas those to the north and inside UDMA in Chah-Breshk and Tale-Ghorban are basaltic trachyandesites (Fig. 1b).

3- Analytical Methods

About 80 thin sections from the volcanic rocks of the study area were examined under the microscope. Of these a total of twenty selected samples were analyzed for mineral chemistry, whole rock major, trace and rare earth element composition at the Institute of Geosciences of Potsdam University and Geo Forschungs Zentrum (GFZ). Mineral compositions were determined using a Cameca Microbeam electron microprobe on carbon-coated polished sections. The wave dispersive system with crystal spectrometers and for energy dispersive analyses (EDS) a link system with beryllium window, Si (Li) detector and XP3 pulse processor were used. Acceleration voltage was 15 KV. Counting time for individual elements and sample currents were 80s and 7nA, respectively. Whole rocks major and trace element compositions were determined on fused discs using an automated Philips PW1400 XRF spectrometer with a rhodium anode tube. REE content were analyzed by ICP-MS from pulps after 0.25 g samples of rock powder were dissolved by four acid digestions at University of Potsdam. Loss on ignition (LOI) is by weight different after ignition a 1000 °C. Detection limits range from 0.01 to 0.1 wt% for major oxides, 0.1 to 10 ppm for trace elements and 0.01 to 0.5 ppm for the rare earth elements.

Results

4-1 Petrography

The Shahre-Babak Pleistocene basaltic lavas are generally highly porphyritic with a phenocryt content up to 50-60% of the total rock volume and consist mainly of plagioclase, pyroxene and olivine. They are poorly vesicular and show porphyric, microlitic porphyric, hyalo-microlitic porphyric, glomeroporphyritic, fluidal, intergranular and rarely intersertal textures. Pyroxene is by far the most abundant phenocryst phase, followed by olivine. Trachybasaltic rocks consist of clinopyroxene and olivine phenocrysts and contain rare xenoliths consisting an olivine and clinopyroxene cumulate. Basaltic trachyandesitic rocks consist of olivine, clinopyroxene, opacitized amphiboles phenocrysts and few quartz xenocrysts (1-3mm) mantled with clinopyroxene (<0.5 mm wide), the composition of which is similar to those of clinopyroxene phenocrysts of host basalts. Quartz xenocrysts are derived from a separate source and interprted as an evidence of magma mixing or crustal contamination [30, 22]. In both rock types phenocrysts are enclosed within a glassy or fine grained groundmass that contains microlitic plagioclase, Fe-Ti oxide, and opaque minerals. Plagioclase, andesine to labradorite in composition (An_{45-60}), is by far the most abundant phase and occurs mainly as subhedral laths and microlites in the groundmass. The clinopyroxene phenocrysts are euhedral to subhedral Ca-rich crystals, fairly homogeneous in composition ($Wo_{40-47}En_{43-51}Fs_{6-10}$) and can be classified as diopsitic-augite. They are commonly zoned with core rich in MgO and TiO_2, up to 2 and 0.8 wt% respectively and depleted in FeO typically 2 wt% relative to their rims [32]. In a (Ca+Na) versus Ti diagram (Leterrier et al., 1982) that determine alkaline, tholeiitic and calc-alkaline basalts, pyroxenes of both rock types plot in the alkaline field (Fig. 2). Al^{VI}/Al^{IV} in pyroxenes indicates low crystallization pressures [58]. Olivine phenocrysts are typically subhedral, fractured and occasionally show absorbed rims with forsterite contents ranging from 80 to 92 mol%. Some phenocrysts contain small glass and Cr-spinel inclusions and show sign of idingitizitation near the rims (Hosseini, in preparation). The Fe-Ti oxides are magnetite.

4-2 Whole Rock Major and Trace Elements

Rock samples with SiO_2 (45.1-50.6) fall in the trachybasalt, whereas samples with SiO_2 (52.0-54.9) fall in the basaltic trachyandesite on the total alkalis versus silica diagram (TAS diagram, Le Maitre [36], Fig. 3). The volcanic rocks are of mainly alkalic with some tendency toward subalkalic character, based on the classification of Miyashiro [45] (Fig. 3). In P_2O_5 versus Zr diagram for basalts [72] (Fig. 4), all samples plot in the field of alkali basalt. Trachybasalt with high MgO, Cr and Ni contents are less evolved ne-normative olivine basalts, whereas basaltic trachyandesite with higher SiO_2 and Al_2O_3 contents are more evolved hy-normative olivine basalt.

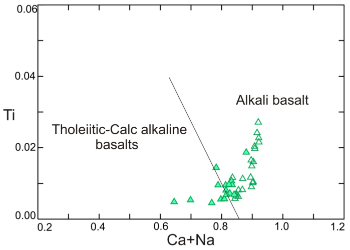

Figure 2. Ti versus (Ca+Na) diagram for clinopyroxene of Shahre-Babak Pleistocene basaltic rocks (after [37]). Δ=Trachybasalt, ▲=Basaltic trachyandesite.

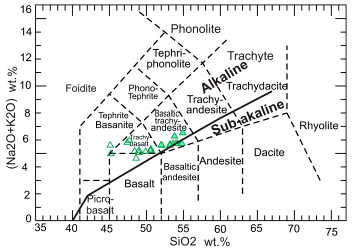

Figure 3. Total alkali vs. silica (TAS) diagram for the Shahre-Babak Pleistocene basaltic rocks (according to [35]) and alkali-subalkali discrimination (curved line according to [44]). Symbols as in Fig. 2.

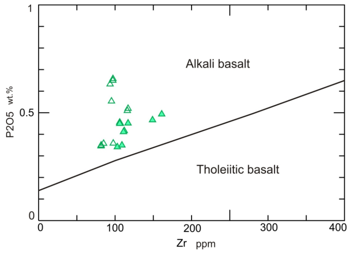

Figure 4. Zr versus P_2O_5 diagram for the Shahre-Babak Pleistocene basaltic rocks illustrating their classification as alkali basalt (after [71]). Symbols as in Fig. 2.

In the Shahre-Babak trachybasalt the MgO, MnO, CaO, FeO and TiO_2 contents are higher than those in basaltic trachyandesites, the total alkali content in both groups are similar (Table 1). However, the basaltic trachyandesites have higher Al_2O_3, SiO_2 and to some extent Na_2O contents than the trachybasalt. There are also pronounced differences between some of the oxide contents in each rock group (Table 1). This can be explained by fractionation of common mineral phases such as clinopyroxene, olivine, hornblende and to minor amounts magnetite. In trachybasalts rocks SiO_2 and Al_2O_3 contents (to some extent Na_2O) increases whereas P_2O_5 and K_2O contents (to some extent MgO and CaO) decrease from Tale-Siah to Khorsand into Chah-Bagh (Table 1). In Khorsand also TiO_2 is higher. In the basaltic trachyandesites TiO_2, CaO and FeO content increases and SiO_2 content (to some extent MgO) decreases from Tale-Ghorban to Chah-Breshk (Table 1). High contents of highly incompatible elements (e.g. Th and Zr) in basaltic trachyandesites relative to trachybasalts and between different outcrops in each group could be due to either differences in degree of partial melting of the source rock and/or a function of fractionation. There is a decrease of FeO, TiO_2, MgO, CaO, MnO, Co, Nb, Ta, and Cr contents, while Al_2O_3, Na_2O, K_2O, P_2O_5, Sr, Ba, Zr, Hf, and Th contents increase with increasing SiO_2 in the basaltic trachyandesites (Fig. 5). In trachybasalts FeO, MgO, CaO, TiO_2, K_2O, P_2O_5, Sr, Zr, Co, Hf, Th, Ba, Nb, Ta, and Cr contents decrease, whereas Al_2O_3, Na_2O, increase with increasing SiO_2 (Fig. 5). In general, increasing concentrations of lithophile elements such as K_2O, and Rb, and decreasing concentrations of compatible elements such as MgO, Ni, and Cr with increasing SiO_2 are related to removal of olivine, clinopyroxene and to minor extent hornblende. Decreasing P_2O_5, TiO_2 and Sr with increasing SiO_2 are probably related to apatite, titanomagnetite, and plagioclase fractionation, respectively [63].

In order to determine the geotectonic environment, trace-element contents of the trachybasalts and basaltic trachyandesites are plotted on Zr/4-Nb*2-Y [44] and Zr/Y versus Ti/Y [49] diagrams. The samples mostly plot in the within-plate field (Fig. 6).

MORB normalized incompatible trace element concentration diagrams for both rock types have been plotted as multi-element pattern in Fig. 7. They show enrichment in large ion lithophile elements (LILE; e.g., Sr, K, Rb and Ba) and light rare earth elements (LREE; e.g., Ce), but depletion in high field strength elements (HFSE; e.g., Ta, Nb, Ti, Zr, Hf and Y) and heavy rare earth elements (HREE; e.g. Yb). Their trace element variations show similar high LILE/HFSE ratios, suggesting that they may be derived from similar parental magma (Fig. 7a, b). Nb, Ta and Ti depletion compares to pattern from subduction related (active) continental margins, where a mantle source can be selectively enriched in LILE by metasomatism of a subduction component and /or crustal contamination and crystal fractionation [47, 50, 65, 11, 63] or post-collisional magmatic rocks [70]. Remarkably, the Shahre-Babak basaltic lavas have Ba/Nb>28 which is the most diagonestic geochemical feature of arc magmas [24].

However, the tectonic evolution of the Zagros orogenic belt of Iran indicate that Late Cenozoic-Early Quaternary volcanism in UDMA took place in a collision setting following the Early Jurassic to Late Miocene NE subduction of the Neo-Tethys (Bitlis-Zagros oceanic crust, [5]) beneath the Sanandaj-Sirjan active continental margin which led to final closure of the Neo-Tethys and finally collision between the Arabian and Central Iranian plates along the Zagros Suture Zone. Regarding the collision related (post-collisional) and within-plate setting of the Shahre-Babak alkaline basalts possible explanations of the enrichment in LILE and LREE relative to Ta and Nb are: (a) presence of a subduction component or the addition of an LILE-enriched, Nb-Ta poor fluid component to the mantle wedge [24, 51], or (b) crustal contamination of mantle-derived magmas during their ascent to the surface through assimilation and fractional crystallization (AFC) and or MASH (melting, assimilation, storage and homogenization) [64, 71, 13, 5, 6]. A plot of Th/Y versus Nb/Y (Fig. 8) is used in order to identify the different source components which have been involved in the petrogenesis of the magmas [70, 62]. Samples from Shahre-Babak Pleistocene basaltic lava flows mostly define a coherent trend, with Th/Nb ratio close to 1.0, which may be attributed to the combined effects of crustal assimilation and fractional crystallization (i.e., AFC). The lack of higher Th/Y ratios similar to those of the oceanic basalt array (MORB+OIB) is strongly indication that metasomatism of the mantle source by subduction fluids carrying a trace element signature of a crustal component did not occur. The increase of Zr/Nb ratio with increasing of silica indicates a progressive magmatic differentiation from trachybasalt towards basaltic trachyandesite and may suggest that crustal contamination has played a significant role in their petrogenesis [70, 62].

4-3 Rare Earth Elements

Chondrite-normalized REE patterns of trachybasalt and basaltic trachyandesite lavas are illustrated in Figure 9. The REE, especially light rare earth elements (LREEs) of all samples are highly enriched, compared to chondrite. Their REE patterns are parallel to each other with $(La/Lu)_N$=11-40, indicating a common origin for both trachybasalts and basaltic trachyandesites rocks. REE distribution pattern do not show Eu anomalies (Fig. 9), suggesting minimal amounts of low-pressure plagioclase fractionation and that plagioclase fractionation. Possible due to high oxygen fugacity plagioclase fractionation was not very important in the evolution of the volcanic rocks [28]. The characteristic of light REE enrichment of the Shahre-Babak basalts relative to MORB indicates derivation from an enriched source. Furthermore, their very steep chondrite-normalized patterns are similar to such from alkali basalts in ocean islands with residual garnet in the source and to intraplate alkali basalts [35,57,15,61,73].

Table 1. Representative whole rock analyses of the Shahre-Babak Pleistocene basaltic rocks. (Note: total Fe as Fe_2O_3)

SAMPLE	**ZCH-1**	**ZCH-4**	**ZCH-6**	**ZCH-10**	**ZK-5**	**ZK-7**	**ZS-1**	**ZS-3**	**ZS-8**	**ZS-11**
Area	Chah-bagh	Chah-bagh	Chah-bagh	Chah-bagh	Korsand	Korsand	Takht-siah	Takht-siah	Takht-siah	Takht-siah
Rock type	Trachy basalt	Trachy basalt	Trachy basalt	Trachy basalt	Trachy basalt	Trachy basalt	Trachy basalt	Trachy basalt	Trachy basalt	Trachy basalt
wt%										
SiO_2	49.9	48.6	50.5	50.6	49.0	48.4	45.2	47.7	45.1	47.4
TiO_2	0.932	1.166	0.913	0.925	1.269	1.247	0.914	0.943	0.936	0.951
$Al2O_3$	14.9	14.2	15.3	15.2	14.3	14.1	12.1	12.5	12.6	12.6
Fe_2O_3	8.37	9.13	8.05	8.19	9.17	9.05	7.81	8.03	7.53	8.04
MnO	0.145	0.154	0.139	0.142	0.152	0.151	0.130	0.132	0.130	0.132
MgO	8.76	9.42	7.87	8.46	9.47	9.70	9.38	9.70	6.92	10.39
CaO	9.59	10.44	9.69	9.30	9.57	9.92	13.41	11.39	14.20	11.05
Na_2O	3.94	3.51	4.05	4.11	3.36	3.32	2.85	3.71	3.48	3.47
K_2O	1.19	1.12	1.17	1.20	1.86	1.83	2.12	2.23	2.12	2.33
P_2O_5	0.349	0.358	0.345	0.357	0.519	0.509	0.632	0.649	0.553	0.657
H_2O	0.62	0.84	0.47	0.45	0.59	0.58	1.26	0.99	0.98	0.81
CO_2	0.45	0.55	0.53	0.35	0.30	0.54	2.28	0.55	3.48	0.21
Total	99.1	99.5	99.0	99.3	99.6	99.3	98.1	98.5	98.1	98.1
Or	7	6.5	7	7	11.2	11	13.2	13.5	13.3	14
Qz	0	0	0	0	0	0	0	0	0	0
Ab	30	25	32	32	25	22	4	13	2	12
An	19.5	20	20	19.5	18.5	18	15	11	13.5	12
Ne	3.3	4	2.5	2.8	3.5	5	14.5	13	18.5	12
Di	21	24.5	21	19	22.5	21	40.5	34	46	32
Hy	0	0	0	0	0	0	0	0	0	0
Ol	14.7	15	12.8	14.2	16	16	9	11	1.5	13.5
Mt	2.6	2.8	2.6	2.6	2.9	2.9	2.7	2.6	2.7	2.6
ppm										
Cr	479	506	413	448	527	524	543	566	519	563
Ga	19	21	17	20	19	17	17	17	16	18
Ni	176	147	125	142	182	180	225	232	213	234
V	222	246	229	208	213	211	153	189	172	171
Zn	74	78	75	74	83	81	90	93	83	98
Li	11.5	13.0	11.3	8.18	13.3	10.0	22.5	14.6	16.2	21.8
Co	36.2	38.6	32.6	34.6	38.7	38.5	35.4	36.5	34.8	36.8
Mo	0.77	0.74	0.69	0.61	0.90	1.02	2.42	2.54	2.02	2.83
Cs	0.39	0.39	0.38	0.35	0.66	0.63	0.26	0.74	0.83	0.48
Rb	17.1	15.8	16.6	17.3	37.8	37.7	18.8	21.8	28.2	24.7
Sr	2304	887	1206	1940	656	678	4901	2571	3654	2719
Y	14.4	15.6	14.2	14.7	18.6	18.4	14.2	14.7	14.0	14.5
Zr	81.8	97.6	81.6	85.0	117	116	93.5	97.1	95.3	97.2
Ba	485	491	1156	472	772	734	1717	798	1441	1853
Nb	8.60	12.1	7.43	8.20	18.4	18.4	9.18	9.45	10.1	9.55
Hf	2.39	2.78	2.38	2.44	2.95	3.00	2.58	2.65	2.56	2.68
Ta	0.43	0.66	0.37	0.39	0.95	0.95	0.44	0.48	0.52	0.46
Pb	6.71	6.31	7.29	7.15	5.79	5.70	14.8	15.0	12.5	15.5
Th	2.07	2.24	1.95	2.10	4.25	4.26	6.63	6.78	5.35	6.82
U	0.68	0.66	0.78	0.68	0.95	1.04	1.37	1.33	1.24	1.24
Mg#	0.51	0.51	0.49	0.51	0.51	0.52	0.55	0.55	0.48	0.56
Ba/Nb	56.4	40.5	156	57.6	41.9	39.8	187	84.4	142	194
Ba/Ta	1122	746	3119	1200	809	775	3915	1671	2786	4038
Nb/Y	0.60	0.78	0.52	0.56	0.99	1.00	0.65	0.64	0.72	0.66
Th/Nb	0.24	0.18	0.26	0.26	0.23	0.23	0.72	0.72	0.53	0.71
Th/Y	0.14	0.14	0.14	0.14	0.23	0.23	0.47	0.46	0.38	0.47
Zr/Y	5.69	6.27	5.74	5.79	6.28	6.27	6.60	6.61	6.80	6.68
La	18.4	19.8	18.5	18.9	27.8	27.6	56.3	57.3	45.3	57.7
Ce	40.3	43.7	40.4	41.4	56.4	56.2	117	120	94.2	122
Pr	5.05	5.61	5.05	5.27	6.74	6.72	14.8	15.2	11.7	15.4
Nd	20.4	22.6	20.3	21.2	26.8	26.3	58.5	61.3	46.8	61.3
Sm	3.84	4.28	3.83	3.90	5.01	5.00	9.23	9.64	7.48	9.55
Eu	1.16	1.31	1.21	1.18	1.51	1.52	2.29	2.42	1.98	2.46
Gd	3.37	3.73	3.32	3.35	4.33	4.32	5.41	5.75	4.78	5.58
Tb	0.49	0.54	0.48	0.50	0.64	0.62	0.62	0.64	0.56	0.64
Dy	2.91	3.21	2.85	2.87	3.77	3.75	3.17	3.18	2.97	3.22
Ho	0.59	0.65	0.58	0.59	0.75	0.73	0.57	0.59	0.55	0.59
Er	1.65	1.72	1.61	1.69	2.09	2.02	1.42	1.52	1.47	1.55
Tm	0.23	0.25	0.23	0.22	0.29	0.29	0.21	0.19	0.21	0.20
Yb	1.48	1.59	1.49	1.54	1.83	1.82	1.20	1.25	1.28	1.25
Lu	0.23	0.24	0.23	0.23	0.28	0.27	0.19	0.21	0.18	0.20

Table 1. Continued

SAMPLE	**ZM-1**	**ZM-3**	**ZM-4**	**ZT-2**	**ZT-6**	**ZT-8**	**ZT-10**	**ZR-1**	**ZV-8**	**ZV-12**
Area	Mera	Mera	Mera	Tale-gorban	Tale-gorban	Tale-gorban	Tale-gorban	Chah-breshk	Chah-breshek	Chah-breshek
Rock type	Basaltic trachy andesite	Basaltic trachy andesite	Basaltic trachy andesite	Basaltic trachy andesite	Basaltic trachy andesite	Basaltic trachy andesite	Basaltic trachy andesite	Basaltic trachy andesite	Basaltic trachy andesite	Basaltic trachy andesite
wt%										
SiO_2	53.6	53.2	54.2	54.9	53.8	54.8	54.0	53.2	52.1	52.0
TiO_2	0.869	0.865	0.857	0.866	0.820	0.777	0.785	0.994	0.983	0.965
Al_2O_3	15.3	15.2	15.2	15.8	15.7	16.9	16.9	16.1	15.9	15.8
Fe_2O_3	7.22	7.13	7.17	6.52	6.52	6.75	6.63	7.33	7.47	7.37
MnO	0.121	0.119	0.122	0.116	0.115	0.125	0.124	0.107	0.132	0.129
MgO	7.43	7.15	7.67	5.22	5.72	5.99	4.87	5.27	6.06	6.02
CaO	8.21	8.64	7.94	7.80	8.50	7.74	8.83	8.78	9.22	9.35
Na_2O	3.93	3.91	3.94	4.17	4.15	4.34	4.38	3.82	3.93	3.93
K_2O	1.79	1.75	1.77	2.34	2.12	1.38	1.34	1.78	1.65	1.68
P_2O_5	0.455	0.450	0.449	0.493	0.466	0.349	0.341	0.451	0.416	0.411
H_2O	0.34	0.45	0.29	0.80	0.54	0.48	0.64	1.02	0.93	0.89
CO_2	0.13	0.53	0.06	0.18	0.54	0.05	0.78	0.25	0.88	0.96
Total	99.5	99.4	99.6	99.2	99.0	99.6	99.5	99.1	99.6	99.6
Or	10.5	10.5	10.5	14	12.8	8	8	11	10	10
Qz	0	0	0	1	0	1	0.5	1	0	0
Ab	35.5	35.5	35	38	38	39	40	35	36	36
An	18	19	18	18	18.2	21	23	22	21	20.5
Ne	0	0	0	0	0	0	0	0	0	0
Di	15.2	17	14.2	14.7	17	11	15.8	16	18	19
Hy	11	9	14.5	10.5	6.8	15	9.5	11	5.2	3
Ol	4.8	5	3	0	3.2	0	0	0	5.5	6.5
Mt	2.5	2.5	2.5	2.5	2.5	2.4	2.4	2.7	2.7	2.6
ppm										
Cr	322	322	331	216	233	212	166	324	328	328
Ga	18	22	20	22	20	20	20	19	21	22
Ni	174	179	194	120	127	94	50	94	141	132
V	139	142	154	172	154	167	146	213	205	192
Zn	78	77	78	77	74	79	78	85	76	74
Li	11.2	11.7	11.5	13.0	10.9	10.5	10.8	9.84	9.58	10.2
Co	30.0	29.3	30.1	24.0	24.6	23.6	21.6	23.7	28.9	28.7
Mo	0.84	0.83	0.81	1.25	1.13	0.77	0.38	1.36	0.90	0.73
Cs	0.70	0.65	0.74	0.76	0.60	0.80	0.30	1.22	0.47	0.34
Rb	30.8	29.7	31.9	36.0	32.5	23.5	16.8	30.6	28.6	28.4
Sr	1839	1252	980	1691	2083	954	1149	995	881	898
Y	13.9	13.8	13.8	15.1	14.7	14.1	12.7	15.6	14.6	14.8
Zr	106	107	106	161	149	109	103	117	112	111
Ba	615	707	573	1016	940	502	482	752	618	655
Nb	8.66	8.68	8.66	8.60	8.45	6.91	6.03	11.6	10.7	10.4
Hf	2.82	2.90	2.84	4.48	4.10	3.06	3.03	3.18	3.04	2.99
Ta	0.44	0.45	0.43	0.38	0.39	0.36	0.31	0.63	0.57	0.57
Pb	9.53	9.53	9.17	12.9	11.4	9.54	10.4	7.59	7.34	8.28
Th	5.67	5.61	5.58	10.1	9.76	4.50	4.54	4.71	4.29	4.34
U	1.90	1.75	1.68	2.87	2.78	1.53	1.38	1.56	1.30	1.52
Mg#	0.51	0.50	0.52	0.44	0.47	0.47	0.42	0.42	0.45	0.45
Ba/Nb	71.0	81.5	66.1	118	111	72.6	79.9	64.6	57.8	63.0
Ba/Ta	1410	1563	1343	2673	2404	1400	1531	1191	1086	1158
Nb/Y	0.62	0.63	0.63	0.57	0.57	0.49	0.47	0.74	0.73	0.70
Th/Nb	0.66	0.65	0.64	1.17	1.16	0.65	0.75	0.41	0.40	0.42
Th/Y	0.41	0.41	0.41	0.67	0.66	0.32	0.36	0.30	0.29	0.29
Zr/Y	7.60	7.71	7.66	10.6	10.1	7.72	8.05	7.46	7.67	7.48
La	31.0	31.5	30.9	45.3	43.2	26.7	25.2	28.4	26.6	26.6
Ce	61.3	62.3	60.7	86.4	82.3	54.0	50.5	56.9	54.4	54.5
Pr	7.43	7.48	7.40	10.1	9.45	6.68	6.22	7.12	6.70	6.60
Nd	29.5	29.6	29.4	38.5	36.6	26.7	25.0	28.0	26.4	26.4
Sm	5.38	5.54	5.54	6.48	6.20	5.04	4.82	5.16	4.88	4.99
Eu	1.58	1.59	1.59	1.81	1.70	1.49	1.44	1.46	1.48	1.48
Gd	4.11	4.24	4.14	4.69	4.37	4.05	3.78	4.09	3.91	4.00
Tb	0.54	0.57	0.53	0.60	0.56	0.52	0.51	0.58	0.54	0.53
Dy	2.99	2.98	2.93	3.15	3.13	2.92	2.74	3.24	3.02	3.06
Ho	0.56	0.54	0.54	0.59	0.56	0.57	0.52	0.60	0.59	0.58
Er	1.42	1.49	1.38	1.56	1.58	1.48	1.39	1.62	1.56	1.54
Tm	0.20	0.21	0.20	0.22	0.20	0.20	0.19	0.22	0.22	0.21
Yb	1.21	1.24	1.21	1.37	1.35	1.30	1.25	1.48	1.43	1.43
Lu	0.18	0.19	0.19	0.20	0.19	0.19	0.19	0.22	0.20	0.20

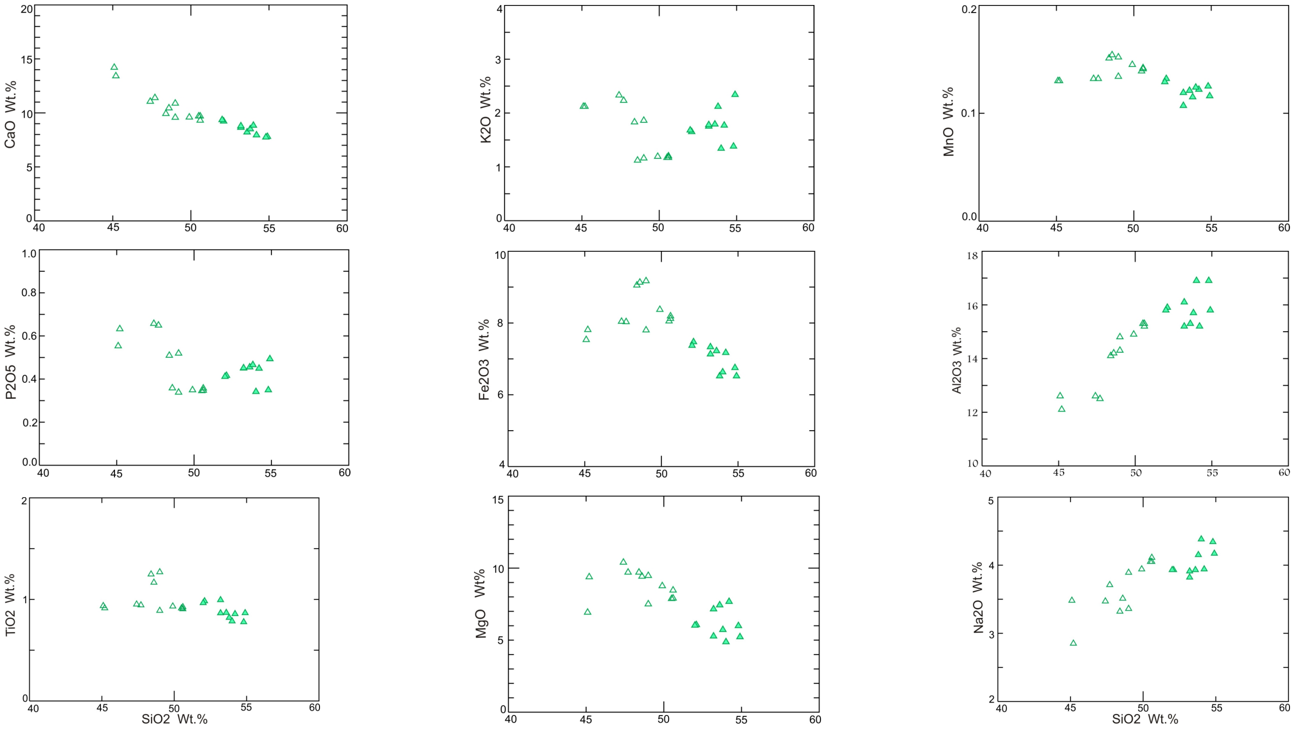

Figure 5. (a). Variation diagrams of selected (a) major and (b) trace elements versus silica for the Shahre-Babak Pleistocene basaltic rocks. Symbols as in Fig. 2.

Discussion

It is generally argued that Urumieh-Dokhtar magmatic assemblage represents the magmatic arc overlying the slab of Neo-Tethyan ocean lithosphere which was subducted northwards beneath the Iranian plate. Generation of magmas from a depleted mantle source and/or their emplacement within continental crust with variable degrees of contamination and fractional crystallization has been related to a detached sinking slab following Miocene continental collision along the Zagros Suture Zone [8, 3]. However different origins have been proposed for the Pleistocene alkaline and calc-alkaline volcanism in the UDMA of Iran. Slab breakoff, the detachment of oceanic lithosphere from continental lithosphere during or after continental collision can explain the presence of mantle signatures in plutonic and volcanic rocks by input of heat from the asthenosphere (e.g., [26, 16]). This can be confirmed by presence of adakitic magmatism in UDMA [16]. This thermal consequence allows sufficient thermal perturbation to melt metasomatised mantle lithosphere [17]. Additionally Berberian and King [9] related them this thermal perturbation to deep sited strike slip faulting. According to major, minor and trace element concentrations, the Shahre-Babak alkaline basaltic rocks show characteristic of subduction related (active) continental margins, OIB's and within-plate tectonic environments. They lie in the within-plate fields on the discrimination diagrams [44, 49]. Considering the timing of collision between the Arabian and Central Iranian plates along the Bitlis-Zagros suture zone during Late Miocenee [33] or Late Eocene [48], we deduce a collision related (Post-collisional) and within-plate setting for the Pleistocene Shahre-Babak alkaline basalt. Both trachybasalt and basaltic trachyandesite trace element variations are similar to each other, with high LILE/HFSE ratios, suggesting that they were derived from a common parental magma. Enrichment in LILE and LREE relative to Ta, Nb and Ti can be explained by crustal contamination (not related to subduction processes) through assimilation and fractional crystallization (AFC, [19]) and /or MASH (melting, assimilation, storage and homogenization [5]. The degree of contamination varies between trachybasalts and basaltic trachyandesites. Spider diagrams show pattern similar to the Red Sea [7] and Rio Grand Rift [27] pattern. Products of these volcanic suites were formed by partial melting of mantle sources and emplaced during continental rifting. The variations in incompatible elements (i.e., enrichments of K, Rb, Ba) suggest that open system processes operated during

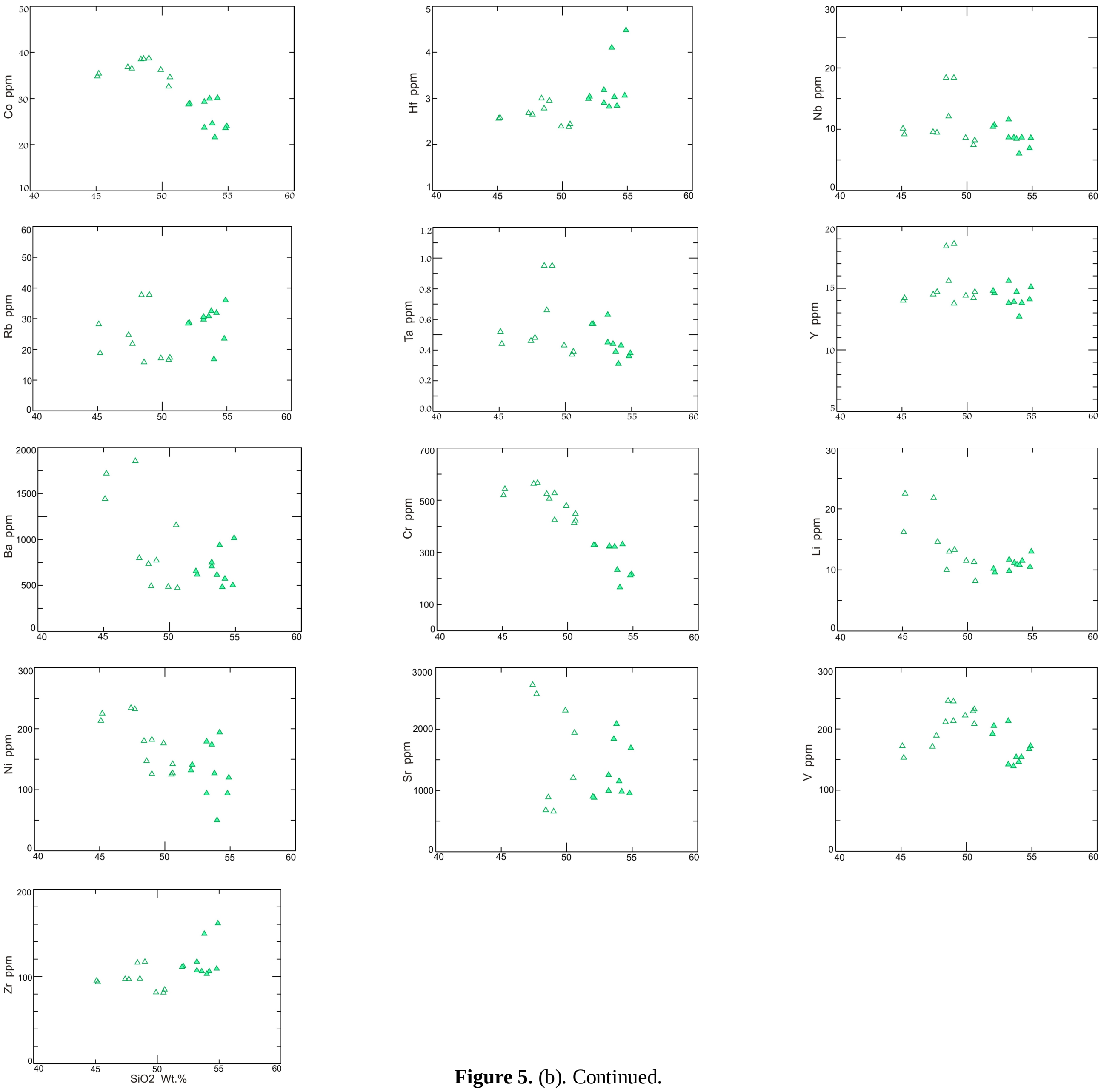

Figure 5. (b). Continued.

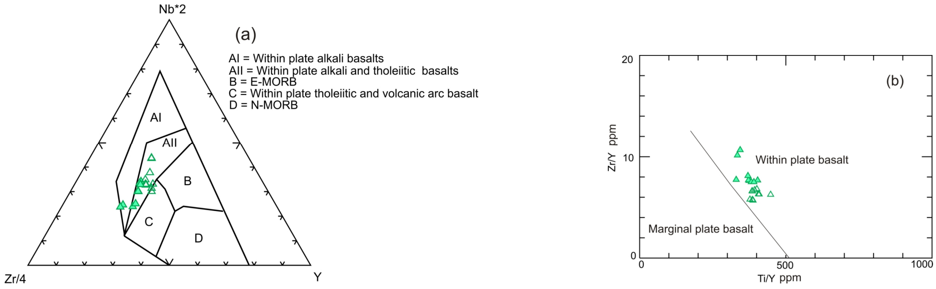

Figure 6. Tectonic environment discrimination diagrams of the Shahre-Babak Pleistocene basaltic rocks (Zr-Nb-Y, after [43]; Zr/Y versus Ti/Y, after [48]). Symbols as in Fig. 2.

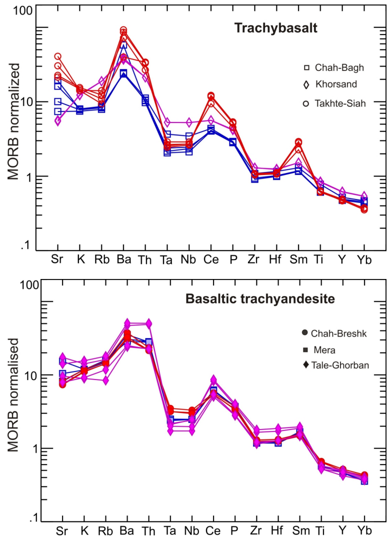

Figure 7. Multielement spider patterns for the Shahre-Babak Pleistocene basaltic rocks, normalized to MORB (normalization constants from [46]). Symbols as in Fig. 2.

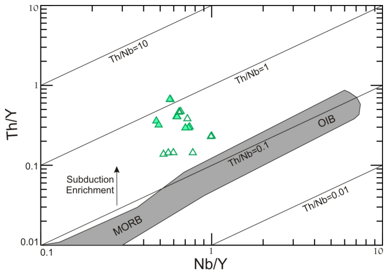

Figure 8. Th/Y versus Nb/Y for the Shahre-Babak Pleistocene basaltic rocks compared to the range of variation in mid-ocean ridge basalts (MORB) and ocean island basalts (OIB) (after [61]). Symbols as in Fig. 2.

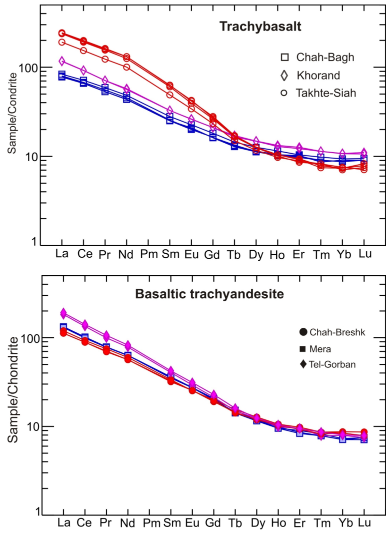

Figure 9. Chondrite-normalized REE diagrams for the Shahre-Babak Pleistocene basaltic rocks. Symbols as in Fig. 2.

formation of the Shahre-Babak Pleistocene alkaline basaltic rocks. They formed from magmas originated in the mantle and were affected by assimilation and contamination processes during ascent through the crust. The fact that Shahre-Babak Pleistocene alkaline basaltic rocks situated between two NW-SE running right lateral strike slip faults (Rafsanjan and Dehshir faults) point to the fact that ascent and eruption of these magmas, originated in the mantle, and was probably controlled by the fault zone, which probably reaches deep down to the base of lithosphere.

Acknowledgements

Financial support for all analyses was provided by Department of Geology of Potsdam University in Germany. S. Zia Hosseini would like to express his gratitude to Drs. Uwe Altenberger and Martin Ziemann for their help and advice on interpretation of data. He also thanks Antje Musiol and Christine Frscher of the institute at Potsdam University for their helps in the laboratories.

References

1. Agard, P., Omrani, J., Jolivet, L. & Mouthereau, F. Convergence history across Zagros (Iran): constraints from collisional and earlier deformation, *Int. J. Earth Sci.*, **94**: 401-419 (2005).
2. Ahmad, T., Posht Kuhi, M. Geochemistry and petrogenesis of Urumiah- Dokhtar volcanic belt around Nain and Rafsanjan areas: a preliminary study. Treatise on the geology of Iran , Iranian Ministry of Mines and Metals, 90 p (1993).
3. Alavi, M. Tectonics of the Zagros orogenic belt of Iran: new data and interpretations, *Tectonophysics.*, **229:** 211-238 (1994).
4. Alavi, M. Regional stratigraphy of the Zagros fold-thrust belt of Iran and its proforeland and evolution, *Am. J. Sci*., **304**: 1-20 (2004).
5. Aldanmaz, E., Pearce, J.A., Thirlwall, M.F., Mitchell, J.G. Petrogenesis evolution of late Cenozoic, post-collision volcanism in western Anatolia, Turkey. *J. Volcanol. Geotherm. Res.*, **102**: 67-95 (2000).
6. Alici, P., Temel, A., Gourgaud, A., Vidal, P. & G¨undo˘gdu, M. N. Quaternary Tholeiitic to Alkaline Volcanism in the Karasu Valley, Dead Sea Rift Zone, southeast Turkey: Sr–Nd–Pb–O isotopic and trace element approaches to crust mantle interaction. *Int. Geol. Rev.*, **43**(2): 120-138 (2001).
7. Altherr , R., Henjes- Kunst, F., Puchelt, H., and Baumann, A., Volcanic activity in the Red sea axial trough-evidence for a large mantle diapir, *Tectonophysics*, **150**: 121-133 (1988).
8. Berberian, F., Berberian, M. Tectono-plutonic episodes in Iran. In: Gupta, H. K., Delany,F.M. (Eds), Zagros, Hindukosh, Himalaya. Geodynamic Evolution. *Am. Geophy. Union*, Washigton, DC, pp. 5-32 (1981).
9. Berberian, M., King, G.C.P. Towards a paleogeography and tectonic evolution of Iran, *Can. J. Earth Sci.,* **18:**

210-265 (1981).

10. Berbberian, F., Muir, I.D., Pankhurst, R.J., Berbberian, M. Late Cretaceous and early Miocene Andian type plutonic activitiy in northern Makran and Central Iran. *J. Geol. Soc. London*, **139**: 605-614 (1982).
11. Bindeman, I.N., Eiler, J.M., Yogodzinski, G., Tatsumi, Y., Stern, C., Grove, T., Portnyagin, M., Hoernle, K., Danyushevsky, L. Oxygen isotope evidence for slab melting in modern and ancient subduction zones. *Earth Planet. Sci. Lett.*, **235**: 436-480 (2005).
12. Borg, L.E., Clynne, M.A., Bullen, T.D. The variable role of slab derived fluids in the generation of a suite of primitive calc-alkaline lavas from the southern most Cascades, California. *Can. Mineral.*, **35**: 425-452 (1997).
13. Buket, E, Temel, A. Major-element, trace-element, and Sr-Nd isotopic geochemistry and genesis of Varto (Mus) volcanic rocks, Eastern Turkey. *J. Volcanol. Geotherm. Res.*, **85**: 405-422 (1998).
14. Churikova, T., Dorendorf, F., Worner, G. Sources and fluids in the mantle wedge below Kamchatka, evidence from across-arc geochemical variation. *J. Petrol.*, **42**: 1567-1593 (2001).
15. Clague, D. A. & Frey, F. A. Petrology and trace element geochemistry of the Honolulu Volcanics, Oahu: implications for the oceanic mantle below Hawaii. *J. Petrol.*, **23**: 447-504 (1982).
16. Dargahi, S. Post-collisional Miocene magmatism in the Sarcheshmeh-Shahrebabak region NW of Kerman: Isotopic study, petrogenetic analysis and geodynamic pattern of granitoid intrusives and the role of adakitic magmatism in development of copper minralization. Unpublished Ph.D. thesis, Shahid Bahonar University of Kerman, 310 p (2007).
17. Davies, J.H., von Blanckenburg, F. Slab breakoff: A model of lithosphere detachment and its test in the magmatism and deformation of collisional orogens. *Earth Planet. Sci. Lett.*, 129: 85-102 (1995).
18. Dehghani, G. A., Makris, T. The gravity fieldand crustal structure of Iran. *Neu. Jahrab.Geol. Palaont. Abh.*, **168** (2-3): 215-229 (1984).
19. DePaolo, D.J. Trace element and isotopic effects of combined wallrock assimilation and fractional crystallization. *Earth Planet. Sci. Lett.*, **53**: 189-202 (1981).
20. Dimitrijevic, M.D. Geology of kerman region. Geol. Surv. Iran, Yu/52, 334 p (1973).
21. Elburg, M.A., Bergen, M.V., Hoogewerff, J., Foden, J., Vroon, P., Zulkarnain, I., Nasution, A. Geochemical trends across an arc continental collision zone: magma sources and slab-wedge transfer processes below the Pantar Strait volcanoes, Indonesia. *Geochim. Cosmochim. Acta*, **66**: 2771-2789 (2002).
22. Espinoza, F., Morata, D., Pelleter, E., Maury, R.C., Suárez^{c}, M., Lagabrielle, Y., Polvé^{e,a}, M., Bellon, H., Cotton, J., De la Cruz, R., Guivel, C. Petrogenesis of the Eocene and Mio-Pliocene alkaline basaltic magmatism in Meseta Chile Chico, southern Patagonia, Chile: Evidence for the participation of two slab windows. *Lithos*, **82**: 315-343 (2005).
23. Falcon, N. Southern Iran-Zagros Mountains, *in* Spencer, A. M., editor, Mesozoic-Cenozoic orogenic belts: *Geol. Soc. London Spec.Publ.*, **4**: 199-211 (1974).
24. Fitton, J. G., James, D., Kempton, P. D., Ormerod, D. S. & Leeman, W. P. The role of lithospheric mantle in the generation of Late Cenozoic basic magmas in the western United States. In: Menzies, M.A., Cox, K.G., (Eds.), Oceanic and Continental lithosphere: Similarities and Differences. *J. Petrol.*, Special Lithosphere Issue, pp 331-49 (1988).
25. Forster, H., Fesefeldt, K., Kurster, M. Magmattic and orogenic evolution of the central Iranian volcanic belt. In: 24th International geology congress section 2: 198-210 (1972).
26. Ghasemi, A., Talbot, C.J. A new tectonic scenario for the Sanandaj- Sirjan Zone (Iran). *J. Asian Earth Sci.*, **26**: 683-693 (2006).
27. Gibson, S. A., Thompson, R. N., Leat, P. T., Dickin, A. P., Morrison, M. A., Hendry, G. L. & Mitchell, J. G. Asthenosphere-derived magmatism in the Rio Grande rift: implications for continental break-up. In: Storey, B. C., Alabaster, T., Pankhurst, R. J. (Eds.) *Magmatism and the Causes of Continental Break-up. Geol. Soc. London Spec.Publ.*, **68**: 61-89 (1992).
28. Gill, J.B. Orogenic andesites and plate tectonic. Springer-Verlag, Berlin, 390 p (1981).
29. Grove, T.L., Kinzler, R.J. Petrogenesis of andesites. Annu. Rev. *Earth Planet. Sci*., **14**: 417-454 (1986).
30. Hibbard, M.J. Petrography to petrogenesis. Englewood Cliffs, NJ: Prentice Hall, 587 p (1995).
31. Hofmann, A.W., White, W.M. Mantle plumes from ancient oceanic crust. *Earth Planet. Sci. Lett.*, **57**: 421-436 (1982).
32. Hosseini, S.Z. Mineralogy, Geochemistry and Petrogenesis evolution of Pleistocene basaltic lava flows in the Shahre-Babak area, NW of Kerman, Iran: Implication for the evolution of Urumieh-Dokhtar Magmatic Assemblage. Ph.D. thesis, In preparation (2009).
33. Innocenti, F., Manetti, P., Mazzuuoli, R., Pasquare, G., Villari, Anatolia and North-western Iran. In: Thorpe R.S. (Ed.) Andesite. Wiley, Chichester, pp. 315-349 (1982).
34. Jung, D., Kursten, M., Tarkian, M. Post-Mesozoic volcanism in Iran and its relation to the subduction of the afro-Arabian under the Eurasian plate. In: Pilger, A., Rosler, A. (Eds.), Afar between continental and oceanic rifting. Schweizerbartsche Verlagbuchhand-lung, Stuttgart, pp. 175-181 (1976).
35. Kay RW, Gast PW. The rare earth content and origin of alkali-rich basalts. *J. Geol.*, **81**: 653-682 (1973).
36. Le Maitre, R.W., Streckeisen A., Zanettin, B., Le Bas, .M.J., Bonin, B., Bateman, P. (Eds.), Igneous rocks: A classification and Glossary of Terms: Recommendations of the International Union of Geological Sciences Subcommission on the Systematics of igneous Rocks. Cambridge University Press, Cambridge, 256 p (2005).
37. Lensch, G. (ed.), Plate tectonic, orogeny and mineralization in the Iranian fold belts. *Neu. Jahrab.Geol. Palaont. Abh.*, **168**: 145-568 (1984).
38. Leterrier, J., Maury, R.C., Thonon, P., Girard, D., Marchal, M. Clinopyroxene composition as a method of identification of the magmatic affinities of palaeo-volcanic series. *Earth Planet. Sci. Lett.*, **59**: 139-154 (1982).
39. Marcy, R.C., Defant, M.J., Joron, J.L. Metasomatism of arc mantle inferred from elements in Philippine xenoliths. *Nature*, **360**: 661-663 (1992).
40. McDonough, W.F. Partial melting of subducted oceanic crust and isolation of its residual eclogitic lithology. *Philos. Trans. Royal Soc. London*, **335**A: 407-418 (1991).

41. McKenzie, D.P., O'Nions, R.K. Partial melt distributionfrom inversion of rare earth element concentrations. *J. Petrol*., **32**: 1021-1991 (1991).
42. McKenzie, D.P., O'Nions, R.K., The source regions of OceanIsland Basalts. *J. Petrol*. **36**: 133-159 (1995).
43. McQuarrie, N., Stock, J.M., Verdel, C. & Wernicke, B.P. Cenozoic evolution of Neotethys and implications for the causes of plate motions, *Geophys. Res. Lett.,* **30:** 2036 (2003).
44. Meschede, M. A method of discriminating between different types of mid-ocean ridge basalt and continental tholeiites with the Nb-Zr-Y diagram. *Chem. Geol*., **56**: 207-218 (1986).
45. Miyashiro, Nature of alkalic volcanic rock series. *Contrib. Mineral. Petrol.,* **66**: 91-104 (1978).
46. Paul, A., Kaviani, A., Hatzfeld, D., Vergne, J. & Mokhtari, M. Seismological evidence for crustal-scale thrusting in the Zagros mountain belt (Iran), *Geophys. J. Int.,* **166:** 227-237 (2006).
47. Pearce, J.A.. Role of the sub-continental lithosphere in magma genesis at active continental margins. In: Hawkesworth, C.J., Norry, M.J. (Eds.), Continental Basalts and Mantle Xenoliths, Shiva. Cheshire, UK, 230±249 (1983).
48. Pearce, J.A., Bender, J.F., DeLong, S.E., Kidd, W.S.F., Low, P.J., Guner, Y., Şaroğlu, F., Yilmaz, Y., Moorbath, S., Mitchell, J.J., Genesis of collision volcanism in eastern Anatolia Turkey. *J. Volcanol. Geotherm. Res*., **44**: 189-229 (1990).
49. Pearce, J.A., Gale G.H. Identification of ore-deposition environment from trace element geochemistry of associated igneous host rocks. *Geol. Soc. London Spec. Publ*., **7**: 14-24 (1977).
50. Pearce, J.A., Peate, D.W. Tectonic implications of the composition of volcanic arc magmas. *Annu. Rev. Earth Planet. Sci.,* **23**: 251-285 (1995).
51. Saunders A.D., Norry M.J. and Traney J. Origine of MORB and chemically depleted mantle reservoirs: trace element constraints. *J. Petrol*., Special Lithosphere Issue, pp 415-445 (1988).
52. Schiano, P., Cloochiatti, R., Shimizu, N., Maury, R.C., Jochum, K.P., Hofmann, A.W. Hydrous, silica rich melts in the sub-arc mantle and their relationship with erupted arc lavas. *Nature* **377**: 595-600 (1995).
53. Schroder, J.W., Essai sur la structure de I'Iran. *Ecol. Geol. Helv*., **37**: 37-81 (1944).
54. Sengor, A.M.C. A new modal for the late Paleozoic-Mesozoic tectonic evolution of Iran and implication for Oman. In: Roberson, A.H.F., Srarle, M.P., Ries, A.C. (Eds.), The Geology and Tectonics of the oman region, Geol. *Soc. Londan Spec. Publ.,* **22**: 278-281 (1990).
55. Shahabpour, J. Island-arc affinity of the Central Iranian Volcanic Belt. *J. Asian Earth Sci*., **30**: 652-665 (2007).
56. Shaw, D.M. Trace element fractionation during anatexis. *Geochim. Cosmochim. Acta.,* **34**: 237-243 (1970).
57. Shimizu N, Arculus, RJ. Rare earth element concentrations in a suite of basanitoids and alkali olivine basalts from Grenada, Lesser Antilles. *Contrib. Mineral. Petrol*., 50: 231-240 (1975).
58. Simonetti, A., Shore, M., Bell, K. Diopside phenocrysts from nephelinite lavas, Napak volcano, eastern Uganda: evidence for magma mixing. *Can. Mineral*., **34**: 411-421 (1996).
59. Stocklin, J. Structural history and tectonics of Iran: a review: *Am. Assoc. Petro. Geol. Bull.*, **52**: 1229-58 (1968).
60. Stoneley, R. The geology of the Kuh-e Dalneshin area of Southern Iran, and its bearing on the evolution of Southern Tethys, *J. Geol. Soc. London,* **138:** 509-526 (1981).
61. Sun, S.S., McDonough, W.F. Chemical and isotopic systematics of oceanic basalts: implications for mantle composition and processes. In: Saunders, A.D., Norry, M.J. (Eds.), Magmatism in the Ocean Basins. *Geol. Soc. London Spec. Publ.,* **42**: 313-345 (1989).
62. Tankut, A; Wilson, M; Yihunie, T. Geochemistry and tectonic setting of Teratiary volcanism in the Güvem area, Anatolia, Turkey. *J. Volcanol. Geotherm. Res*., **85**: 285-301 (1998).
63. Temizel, İ; Arslan, M. Petrology and geochemistry of Tertiary volcanic rocks from the İKizce (Ordu) area, NE Turkey:Implications for the evolution of the eastern Pontide paleo-magmatic arc. *J. Asian Earth Sci*., **31**: 439-463 (2008).
64. Thompson, R.N., Morrison, M.A., Hendry, G.L., Parry, S.J. An assessment of the relative roles of crust and mantle in magma genesis: an element approach. *Philos. Trans. Royal Soc. London Ser. A,* **310**: 549-590 (1984).
65. Turner, S.P. On the time-scales of magmatism at island-arc volcanoes. *Philos. Trans. Royal Soc. London Ser. A,* **360**: 2853-2871 (2002).
66. Turner, S.P. Some remarks on magmatic processes beneath island arc volcanoes. Advance in Earth Sciences. Imperial College Press, 131-155 (2005).
67. Vernant, P. Contemporary crustal deformation and plate kinematics in Middle East: constrained by GPS measurements in Iran and northern Oman, *Geophys. J. Int.,* **157:** 381-398 (2004).
68. White, W.M., McKenzie, D.P. Magmatism at rift zones: the generation of volcanic continental margins and flood basalts. *J. Geophys. Res*., **94**: 7685-7729 (1989).
69. White, W.M., Patchett, J. Hf-Nd-Sr isotopes and incompatible element abundances in island arcs: implications for magma origins and crust-mantle evolution. *Earth Planet. Sci. Lett.,* **67**: 167-185 (1984).
70. Wilson, M., Tankut, A., Guleç, N. Tertiary volcanism of the Galatia province, north-west Central Anatolia, Turkey. *Lithos,* **42**: 105-121 (1997).
71. Wilson, M. Igneous petrogensis. A global tectonic approach. Springer, 1 edition, 466 p (2007).
72. Winchester, J., Floyd, P.A. Geochemical discrimination of different magma series and their differentiation products using immobile elements. *Chem. Geol*., **20**: 325-343 (1977).
73. Wittke, J.H., Mack, L.E. OIB-like mantle source for continental alkaline rocks of the Balcones province, Texas: trace elements and isotopic evidence. J. *Geol*., **101**: 333-344 (1993).
74. Zellmer, G.F., Annen, C., Charlier, B.L.A., George, R.M.M., Turner, S.P., Hawkesworth, C.J. Magma evolution and ascent at volcanic arc: constraining petrogenetic processes through rates and chronologies. *J. Volcano. Geotherm. Res*., **140**: 171-191 (2005).